Preliminary evaluation of vacuum desorption efficiency and the influence of vacuum port configuration in a calf-20 VPSA system for CO_2 capture

Watchara Sutaro [1], *Chalita* Ratanatawanate [2], *Chantaraporn* Phalakornkule [1,3,*]

[1]Department of Chemical Engineering, Faculty of Engineering, King Mongkut's University of Technology North Bangkok, Bangkok 10800, Thailand
[2]National Nanotechnology Center, National Science and Technology Development Agency, Bangkok 10800 THAILAND
[3]Research Center for Circular and Product and Energy, King Mongkut's University of Technology North Bangkok, Bangkok 10800 THAILAND

Abstract. Vacuum Pressure Swing Adsorption (VPSA) is a promising, energy-efficient technology for post-combustion CO_2 capture; however, mass-transfer resistance during regeneration often limits its performance. To address this, this study evaluates the CO_2 capture performance of the Metal-Organic Framework (MOF) CALF-20 and optimizes vacuum desorption processes. Breakthrough experiments were conducted on an adsorption column (90 cm in height, 2 cm in diameter) containing 244 g of adsorbent using a gas mixture of 15% CO_2/85% N_2 at 5 NLPM. CALF-20 exhibited a breakthrough time of 374 s, with a saturation adsorption capacity of 1.37 mol CO_2/kg. Furthermore, the influence of vacuum port configuration was investigated using three ports located at 11, 50, and 79 cm from the column bottom. The results demonstrate that switching from the conventional single-bottom port configuration (desorption efficiency, η_{DES} = 79.77%) to the optimized 2-port configuration at the bottom and middle (2-M&B) significantly increased η_{DES} to 93.24%. These findings confirm that strategic port positioning effectively mitigates mass-transfer resistance, providing a critical engineering solution for scaling up high-efficiency MOF-based VPSA systems.

1. Introduction

Climate change, driven by rising atmospheric concentrations of greenhouse gases, particularly carbon dioxide (CO_2), has become a global crisis that requires urgent mitigation. According to the International Energy Agency (IEA), global energy-related CO_2 emissions reached a record high of 37.8 Gt in 2024, underscoring the critical need for immediate decarbonization efforts [1]. Major anthropogenic sources of CO_2 include fossil-fuel power

* Corresponding author: chantaraporn.p@eng.kmutnb.ac.th

plants, industrial processes, and combustion-related activities, such as transportation. These emissions have created a critical need for technologies that can efficiently and economically reduce or capture CO_2.

Currently, CO_2 capture technologies are primarily classified into two main types: chemical absorption with liquid solvents and adsorption with solid sorbents. While chemical absorption (e.g., amine scrubbing) is the most mature technology, it is often hindered by high energy penalties from solvent regeneration, corrosion, and solvent degradation. In contrast, adsorption-based methods have emerged as a promising alternative due to their lower energy requirements, ease of operation, and lack of liquid waste generation.

Common adsorption technologies include Pressure Swing Adsorption (PSA), Temperature Swing Adsorption (TSA), and combined Pressure–Temperature Swing Adsorption (PTSA). However, traditional PSA requires significant compression energy, particularly for low-pressure flue gas streams, whereas TSA is typically limited by long cycle times and high thermal energy demands for regeneration [2]. To address these limitations, Vacuum Pressure Swing Adsorption (VPSA) has gained significant attention as an energy-efficient separation method. Recent comparative studies substantiate the energy efficiency of this approach; while conventional chemical absorption technologies typically consume 0.83–1.11 kWh/kg CO_2 for regeneration, optimized VPSA systems can reduce specific energy consumption to approximately 0.42–0.69 kWh/kg CO_2, depending on the adsorbent material and cycle configuration [3]. The VPSA process operates by adsorbing target gases on selective adsorbents, followed by desorption under vacuum. This technique offers a flexible design that enhances CO_2 capture performance and lower energy consumption compared to established chemical absorption methods.

In the VPSA system, the choice of adsorbent material is crucial to overall process performance. Specifically, the adsorbent must prioritize high CO_2/N_2 selectivity to ensure product purity, rapid adsorption–desorption kinetics to accommodate short cycle times, and robust cyclic stability—particularly against moisture—to maintain performance over long-term operation [4]. While Metal–Organic Frameworks (MOFs) are widely recognized for their tunable nanoporous structures, conventional adsorbents such as Zeolite 13X exhibit significant performance degradation in humid flue gas. Although Zeolite 13X exhibits a high CO_2 capacity under dry conditions, studies indicate that its capacity decreases by more than 90% at relative humidity (RH) as low as 5% due to competitive water adsorption [4].

To address these limitations, CALF-20 (Calgary Framework-20) has been selected for this study to enhance the efficiency of the VPSA process. CALF-20 is a zinc-triazolate MOF that offers a competitive CO_2 working capacity of approximately 2.4–2.5 mmol/g (at 0.15 bar, 30 °C) and an exceptional CO_2/N_2 selectivity of over 200 [5]. Most notably, it distinguishes itself through extraordinary hydrolytic stability; experimental data confirm that CALF-20 retains its structural integrity and adsorption performance for over 450,000 adsorption–desorption cycles in the presence of steam and acid gases, a durability benchmark that far exceeds typical MOFs, which degrade rapidly under similar conditions [6–8]. Furthermore, CALF-20 offers distinct advantages in scalability and cost-effectiveness, as it can be synthesized from commercially available reagents without requiring expensive linkers.

To achieve optimal VPSA operation, it is necessary to design a systematic operating cycle and position the vacuum ports appropriately, as these factors directly affect key performance indicators, including CO_2 capture efficiency, product purity, and energy consumption [9, 10]. However, the design of an optimized VPSA process remains challenging. The operational cycle must be carefully timed to maximize adsorbent utilization while ensuring effective desorption. Achieving complete recovery of the adsorbed gas (adsorbate) is often limited by vacuum strength and cycle duration, and maintaining a fully leak-free system—especially

around pipelines, joints, and adsorption columns—poses practical difficulties. Additionally, precise control of gas flow distribution throughout the system is required to maintain stable, efficient operation.

In this study, we investigated CO_2 adsorption on the MOF CALF-20, evaluated its performance, and optimized desorption processes. The research includes the performance of breakthrough curves on a single adsorption column containing the MOF CALF-20. While industrial applications typically use multi-bed configurations, single-column breakthrough experiments provide a fundamental basis for determining intrinsic adsorption kinetics, mass-transfer zones (MTZs), and equilibrium parameters, which are essential prerequisites for predicting the dynamic behavior of complex, large-scale VPSA systems [11]. The study quantifies key adsorption parameters, including breakthrough and saturation adsorption capacities, for a gas mixture of 15% CO_2 and 85% N_2 delivered at a constant pressure of 110 kPa. These specific compositions and pressures were selected to simulate typical post-combustion flue-gas conditions from coal-fired power plants, which generally contain 12–15% CO_2 and operate at near-atmospheric pressure [12]. By replicating these industrial conditions, the study ensures that the observed adsorption behaviors and capacity limits are directly applicable to real-world capture scenarios.

In addition, CO_2 desorption under vacuum through three ports located at 11, 50, and 79 cm from the bottom of the adsorption column was investigated. The underlying physical rationale for selecting these specific port locations is to analyze and mitigate the internal pressure drop gradient along the packed bed during the rapid evacuation phase. In taller or larger-scale industrial columns, excessive pressure drop can create "dead zones" that hinder desorption; thus, optimizing port configuration is critical to ensure uniform pressure distribution and maximize effective working capacity [11]. Different port configurations—port locations (top, middle, bottom) and combinations of these three ports (1-port, 2-port, and 3-port)—were examined to assess their impact on CO_2 purity, flow rate, and desorption efficiency. Crucially, the observed improvements in desorption rates and product purity in this study are analyzed to understand their translation into overall VPSA process performance, specifically targeting the reduction of cycle time and vacuum pump duty, which are the primary drivers of specific energy consumption (kWh/kg CO_2) in CO_2 capture operations [3].

2. Experimental Methodology

2.1 Materials

The MOF CALF-20, supported by the National Nanotechnology Center (NANOTEC), Thailand, was selected for its superior hydrolytic stability and scalability relative to conventional adsorbents [6]. The material was supplied as 3 mm spherical pellets (bulk density: 562 ± 5 kg/m³; average pore diameter: 1.54 nm), a size chosen to optimize the trade-off between column pressure drop and mass-transfer kinetics. Before experiments, the adsorbent was activated at 150 °C under N_2 flow (99.999%, 100 NL/h) for 12 h. This protocol ensures complete regeneration without structural compromise, consistent with established stability benchmarks [7, 8].

2.2 Experimental Apparatus

The experimental apparatus was designed as a single-column VPSA system, consisting of three main parts: (1) the feed unit, (2) the adsorption column unit, and (3) the vacuum

desorption unit. The entire system was assembled according to the schematic diagram shown in Fig. 1.

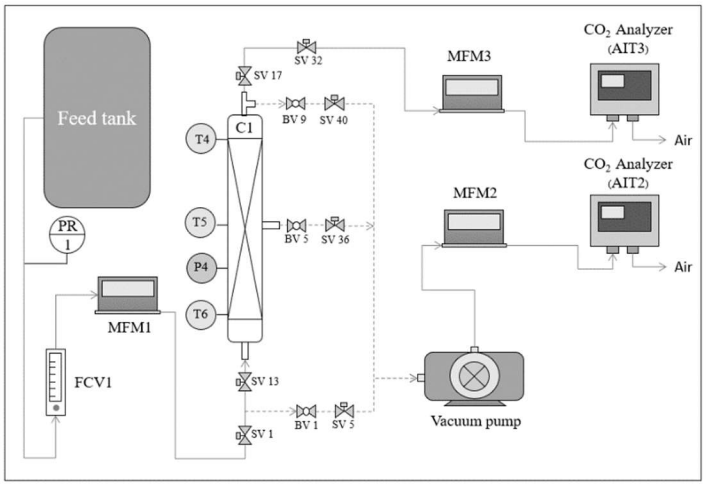

Fig. 1. The setup of the single column adsorption-desorption system (BV: ball valve; C1: column; AIT: CO_2 analyzer; FCV: flow control valve; MFM: mass flow meter; NV: needle valve; P4: pressure transmitter; PR: pressure regulator; SV: solenoid valve; T4, T5, T6: temperature sensor).

2.2.1 Adsorption Unit

A CO_2/ N_2 gas mixture (15/85 %vol) is delivered from the feed tank through a pressure regulator (PR1, SMC™ Model AR20-02-BG-A) to maintain a constant gas pressure of 110 kPa. The gas then passes through a flow control valve (FCV1, Dwyer™ Model VFA-21-SSV) to set the flow rate to a constant 5 NL/min, and through a mass flow meter (MFM1, Bronkhorst™ EL-FLOW Select) to measure the actual gas flow rate. Following this, the gas mixture passes through SV1 and SV13 into the base of the adsorption column (C1). The column is made of unplasticized polyvinyl chloride (UPVC) with an inner diameter of 0.02 m and a height of 0.9 m, and is packed with 244 g of CALF-20 adsorbent. The column is equipped with temperature monitoring devices, thermocouples (T4, T5, T6; KEJUN™ Type K), at heights of 0.11, 0.50, and 0.79 m from the column base, and a pressure transmitter (P4, DUOC™ PT-100, 4–20 mA, 24 VDC) to measure the internal column pressure. The gas exits the top of the column through valves SV17 and SV32, then enters a mass flow meter (MFM3, Bronkhorst™ EL-FLOW Select) and a CO_2 analyzer (AIT3, Guardian™ NGDC Model 200892) to measure the outlet CO_2 concentration.

2.2.2 Desorption Unit

Once the adsorption column is saturated, the feed-side valves (SV1, SV17, SV32) are closed. The system then switches to desorption mode by opening the designated vacuum valves. Vacuum pressure is generated by a vacuum pump (WOOSUNG™ Model MVP-6, 0.37 kW, 220 VAC, 50 Hz, two-stage rotary vane). This pump is connected via valves to draw gas from various ports on the column, which include: the bottom port at the column base (via BV1, SV5), the middle port at a height of 0.4 m from the column base (via BV5, SV36), the top port at a height of 0.9 m from the column base (via BV9, SV40). The desorbed gas flows through a mass flow meter (MFM2, Bronkhorst™ EL-FLOW Select) and enters a CO_2

Analyzer (AIT2, Guardian™ NGDC Model 200892) to measure the concentration of the desorbed CO_2 gas.

2.3 Experimental Procedure

The adsorption step involves feeding a CO_2/N_2 gas mixture (15/85 %vol) from the feed tank into the system via PR1, FCV1, and MFM1. The flow rate is set to a constant 5 NL/min, and the pressure is set to 110 kPa. Valves SV1 and SV13 are then opened to allow the gas to enter the base of column C1. The gas flows through the column and exits at the top, passing to MFM3 and AIT3 until saturation is reached ($C_{out} \approx C_{in}$). During this period, the outlet CO_2 concentration, gas flow rate, pressure (P4), and temperatures (T4–T6) are recorded. The results are used to plot the breakthrough curve and calculate the breakthrough adsorption capacity (q_{BC}) and the saturation adsorption capacity (q_{SC}).

$$q_{BC} = \frac{Q_F X_{CO2}}{22.4 m_{ads}} \left(t_b - \int_{t_0}^{t_b} \frac{C_{t,CO2}}{C_{0,CO2}} dt\right) \ (\text{mol}_{CO2}/\text{kg adsorbent}) \quad (1)$$

$$q_{SC} = \frac{Q_F X_{CO2}}{22.4 m_{ads}} \left(t_s - \int_{t_0}^{t_s} \frac{C_{t,CO2}}{C_{0,CO2}} dt\right) \ (\text{mol}_{CO2}/\text{kg adsorbent}) \quad (2)$$

where, Q_F is the inlet flow rate (L/sec), X_{CO2} is the mole fraction of CO_2 (mol_{CO2}/mol_{total}), m_{ad} is the mass of adsorbent (kg), t_b is the breakthrough time (s), t_s is the saturation time (s), $C_{t,CO2}$ is the outlet CO_2 concentration at any time t (mol_{CO2}/mol_{total}), $C_{0,CO2}$ is the inlet CO_2 concentration (mol_{CO2}/mol_{total}).

After the column is saturated, the feed valves (SV1, SV13) are closed. The designated vacuum valves are opened, and the vacuum pump is activated for 3,600 s to perform desorption under the following configurations.

Desorption via one port located at the bottom (1-Bottom) by opening BV1 and SV5

Desorption via one port located at the middle position (1-Middle) by opening BV5 and SV36

Desorption via one port located at the top position (1-Top) by opening BV9 and SV40

Desorption via two ports located at the middle and bottom positions (2-M&B) by opening BV1, BV5, SV5, and SV36

Desorption via two ports located at the top and bottom positions (2-T&B) by opening BV1, BV9, SV5, and SV40

Desorption via two ports located at the top and middle positions (2-T&M) by opening BV5, BV9, SV36, and SV40

Desorption via three ports located at the top, middle, and bottom positions (3-TMB) by opening BV1, BV5, BV9, SV5, SV36, and SV40.

For each condition, the CO_2 concentration via AIT2 and the gas flow rate via MFM2 are recorded throughout the desorption period. The recorded data is then used to calculate the total amount of CO_2 desorbed ($n_{CO2,EV}$).

$$\dot{n}_{CO2}(t) = x_{CO2}(t) \cdot \frac{Q_{EV}(t)}{22.414} \quad (\text{mol/s}) \quad (3)$$

$$n_{CO2,EV} = \int_0^{t_{EV}} \dot{n}_{CO2}(t)dt \quad (\text{mol}) \quad (4)$$

Where, $\dot{n}_{CO2}(t)$ is the CO_2 desorption rate at time t (mol/s), $x_{CO2}(t)$ is the mole fraction of CO_2 measured at the outlet at time t (mol_{CO2}/mol_{total}), $Q_{EV}(t)$ is the total gas flow rate at the evacuation outlet at time t (L/s (at Normal)), $n_{CO2,EV}$ is the total moles of CO_2 desorbed by evacuation for the entire cycle (mol), and t_{EV} is thedesorption time (s) (3600 s). These

values are then used to calculate the evacuation desorption capacity (q_{EV}) and the evacuation desorption efficiency (η_{DES}) to compare and determine the best desorption method.

$$q_{EV} = \frac{n_{CO2,EV}}{m_{ads}} \ (mol_{CO2}/kg_{adsorbent}) \quad (5)$$

$$\eta_{DES} = \frac{q_{EV}}{q_{SC}} \times 100 \ (\%) \quad (6)$$

where, q_{EV} is the evacuation desorption capacity ($mol_{CO2}/kg_{adsorbent}$), m_{ads} is the mass of CALF-20 adsorbent used in the experiment (kg), η_{DES} is the evacuation desorption efficiency (%), q_{SC} is the saturation adsorption capacity (obtained from the adsorption capacity test) ($mol_{CO2}/kg_{adsorbent}$). Additionally, calculations are performed to determine the CO_2 purity of the desorbed gas and to compare the product purity from each desorption port.

$$CO_2 \text{ purity } (Pu_{CO2,HP}) = \frac{n_{CO2,EV}}{n_{total,EV}} \times 100\% \ (\%) \quad (7)$$

Where $n_{CO2,EV}$ is the total moles of CO_2 desorbed by evacuation for the entire cycle (mol), $n_{total,EV}$ is the total moles of gas desorbed by evacuation for the whole of the cycle (mol), $n_{CO2,feed}$ is the total moles of CO_2 fed during the adsorption step of the cycle (mol).

3. Results and Discussion

3.1 Adsorption study

The breakthrough curve results are shown in Fig. 2. The CO_2 breakthrough curve was measured under dynamic conditions, using a gas mixture of 15% CO_2/85 % N_2 at 110 kPa and a flow rate of 5 NL/min. The results are compared with the Yoon–Nelson model. This semi-empirical model was specifically selected over other kinetic models (e.g., Thomas or Bohart–Adams) due to its simplicity and robustness in predicting the 50% breakthrough time (τ) without requiring detailed physicochemical parameters of the adsorbent bed, such as effective diffusivity or axial dispersion coefficients [13]. While Bohart–Adams is typically limited to the initial breakthrough region and Thomas assumes ideal Langmuir kinetics, Yoon–Nelson provides a superior fit for the entire breakthrough range in binary gas systems [14].

The experimental results (black line) indicate that the breakthrough begins at approximately 400 s, followed by a rapid increase in the outlet concentration to a near-saturation level of 15% CO_2 at approximately 2500 s. The graph profile shows a gradual slope during the breakthrough phase rather than the sharp transition predicted by the model. This is attributed to physical mass transfer resistances, particularly intraparticle diffusion. The observation of this tailing effect is strongly supported by material characterization data, which indicate that CALF-20 has a narrow average pore diameter of 1.54 nm. This microporous structure inherently restricts gas-molecule diffusion into the internal pore network, creating a diffusion-limited regime that prevents instantaneous saturation and results in the observed prolonged tailing behavior [8].

Despite this deviation in the tailing region, the Yoon–Nelson model provides a statistically significant fit for the kinetic region. The calculated rate constant (k_{YN}) was found to be 2.1177 min^{-1}, and the time required for 50% breakthrough (τ) was determined to be 7.97 min. Quantitative analysis confirms the agreement between the model and experimental data, yielding a high coefficient of determination (R^2) of 0.9099 and a Root Mean Square Error (RMSE) of 0.3526. This indicates that the model is reliable for predicting the

approximate start of the breakthrough cycle and the critical saturation midpoint, which are the essential parameters for designing the VPSA cycle time. Based on the good agreement between the experimental results and the model, it can be concluded that CALF-20 has high potential for CO_2 adsorption at flue gas concentrations (15%) and exhibits an adsorption–mass transfer process consistent with that observed in industrial packed beds. From the breakthrough curve analysis, the amount of CO_2 adsorbed at saturation (saturated adsorption) was 0.3751 mol/bed. This value will be used to calculate η_{DES} in the next section.

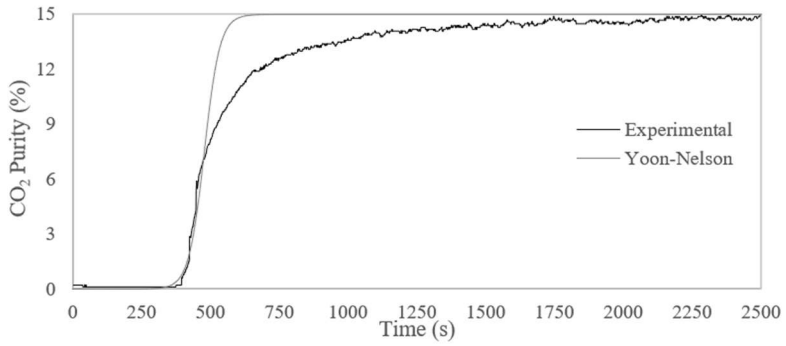

Fig. 2. Comparison of the experimental breakthrough curve for CO_2 on MOF CALF-20 with the Yoon-Nelson model (feed flow rate of 5 NLPM of a gas mixture of 85% N_2 and 15% CO_2).

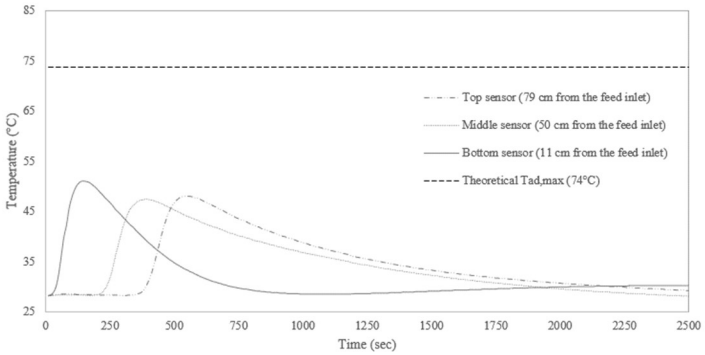

Fig. 3. Experimental temperature profiles at different column locations and the theoretical maximum adiabatic temperature during CO_2 adsorption on MOF CALF-20 (feed flow rate of 5 NLPM of a gas mixture of 85% N_2 and 15% CO_2).

The temperature profile in Fig. 3 shows the temperature changes within the adsorption column, measured by three thermocouples: the bottom sensor (11 cm from the feed inlet), the middle sensor (50 cm), and the top sensor (79 cm). This is shown alongside the theoretical maximum adiabatic temperature line (theoretical $T_{ad,\,max} \approx 74$ °C). The results reflect the characteristic pattern of a thermal adsorption front. The bottom sensor exhibits the earliest peak (~150–200 s), consistent with the feed zone contacting the fully unsaturated adsorbent, which triggers a strong exothermic reaction early in the process. The maximum temperature at the bottom sensor was 51.1 °C, significantly lower than the theoretical $T_{ad,\,max}$ (74 °C), indicating heat loss through the column wall. The middle and top sensors show delayed peaks; the middle sensor peaked at approximately 210–400 s (47.4 °C), and the top sensor peaked at approximately 450–500 s (48.1 °C). This pattern demonstrates the upward

movement of the adsorption heat front through the column, a characteristic of packed-bed adsorption. The peak temperature decreases slightly with height, consistent with heat conduction within the adsorbent material, heat loss at the column walls, and the reduction in the adsorption driving force as saturation is approached. After the peak, the bed temperature gradually cools down as heat dissipates from the column, the adsorption process slows, and the continuous flow of room-temperature feed gas passes through. The final temperature (~27–29 °C) returns to its initial value, indicating that a quasi-steady state is reached after the adsorption phase ends.

This temperature pattern provides evidence supporting that the CALF-20 adsorption process is significantly exothermic. The thermal wave propagates with the mass transfer zone (MTZ) and the onset of CO2 breakthrough, which occurs near the temperature peak observed at the Top sensors. The increased temperature impedes adsorption, reducing adsorption capacity in accordance with Le Châtelier's principle, thereby confirming the tailing observed in the breakthrough test results in Fig. 3.

3.2 Desorption characteristics and the influence of vacuum port configuration

Evacuation desorption tests were conducted under seven vacuum port conditions to evaluate the adsorbent's regeneration performance, starting from a saturated adsorption of 0.3751 mol/bed. The desorption efficiency (η_{DES}) CO_2 purity and desorption energy were calculated and compared in Fig. 4 (a-d).

Desorption efficiency is the primary indicator of the adsorbent's regeneration capability. The experimental results (Fig. 4c) show that multi-way desorption provides a higher η_{DES} than single-way desorption. The 2-M&B configuration achieved the highest desorption efficiency (91.18%), corresponding to the highest amount of CO_2 desorbed ($n_{CO2,\,EV}$), 0.34 mol. Desorption from two ports located at the middle and bottom of the column may reduce flow resistance and increase the mass-transfer driving force, thereby enabling maximum extraction of adsorbed CO_2. In contrast, the 1-Bottom configuration yielded the lowest η_{DES} at 79.77% and the lowest $n_{CO2,\,EV}$ at 0.299 mol, indicating that desorption from a single port at the column base is the least efficient method.

The analysis of CO_2 purity (Fig. 4a) showed that the 1-Middle configuration yielded the highest purity, 84.25%. Meanwhile, the 2-M&B configuration (which had the highest η_{DES}) showed a similar purity of 83.23%. Notably, the 2-T&B configuration yielded the lowest purity of 77.11%. This may be because the Top port draws out inert gas (N_2) and CO2 remaining in the void space at the top of the column during the initial phase of desorption.

The analysis of specific energy consumption for desorption (Fig. 4d) reveals that configurations with high η_{DES} tend to have low specific energy consumption. The 2-T&M configuration, with $\eta_{DES}$of 89.96%, used the lowest specific energy at 24.45 kWh/kg_{CO2}. The 3-TMB and 1-Middle configurations also exhibited very low energy consumption of 24.5 and 24.63 kWh/kg CO_2, respectively. The 1-Bottom configuration, which had the lowest η_{DES}, consumed the highest energy at 28.03 kWh/kg_{CO2}. This result confirms that an appropriate vacuum port design not only enhances desorption efficiency but also significantly helps reduce the energy cost of adsorbent regeneration. The 2-M&B and 2-T&M configurations demonstrate the best balance between high desorption efficiency and low energy cost.

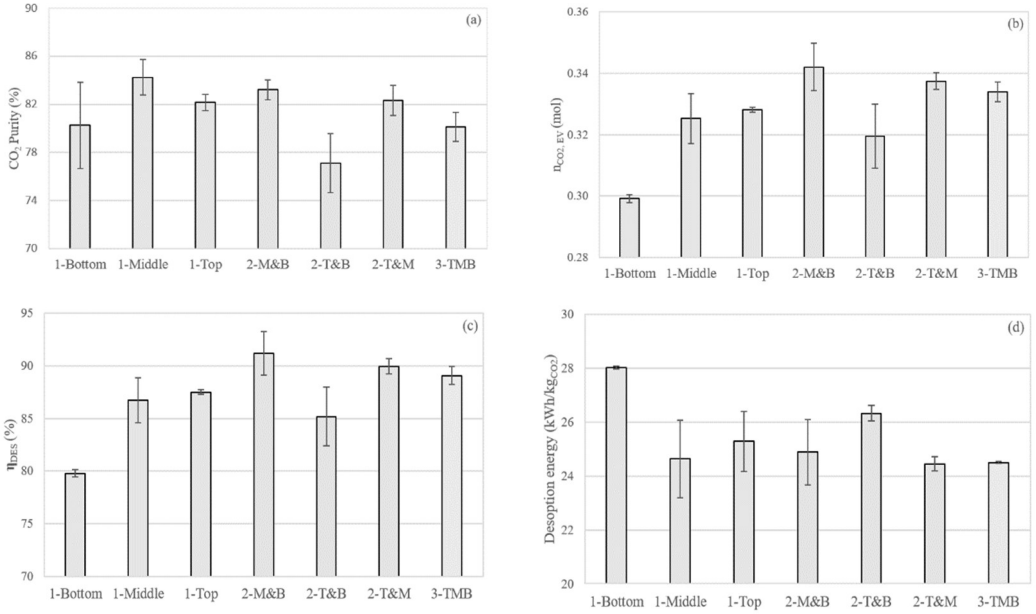

Fig. 4. Comparative desorption performances of different vacuum port configurations: (a) CO_2 purity, (b) total moles of gas CO_2 desorbed ($n_{CO2,\,EV}$), (c) desorption efficiency (η_{DES}), and (d) desorption energy.

4. Conclusions

This study aimed to evaluate the vacuum desorption efficiency and investigate the influence of vacuum port configurations in a VPSA system using CALF-20 adsorbent, providing a basis for efficient VPSA cycle design. Under adsorption conditions, the process of CO_2 adsorption on CALF-20 under dynamic conditions (15% CO_2, 110 kPa) is strongly exothermic, with a maximum measured temperature of 51.1°C. This generated heat directly affects adsorption equilibrium, broadening the mass-transfer zone and causing the adsorbed CO_2 (saturated capacity: 0.3751 mol/bed) to accumulate primarily in the middle and upper sections of the column. Under desorption conditions, the position and number of vacuum ports significantly impact the process performance. The 2-M&B configuration yields the highest desorption efficiency (η_{DES}) at 91.18%. The 2-T&M configuration has the lowest specific energy consumption, at 24.45 kWh/kg CO_2. Conversely, the 1-Bottom configuration (often used in conventional systems) performs the poorest, exhibiting the lowest efficiency (η_{DES} = 79.77%) and the highest energy consumption (28.03 kWh/kg_{CO_2}). The superiority of multi-port strategies (e.g., 2-M&B) is attributed to the reduction of mass-transfer resistance by creating shorter diffusion paths for CO_2 accumulated in the middle and upper parts of the column.

Although these findings are derived from a single-column setup, the fundamental fluid-dynamics and mass-transfer benefits of multi-port desorption are scalable to industrial operations. In fact, in large-scale multi-column VPSA units with high aspect ratios (H/D), the pressure-drop reduction offered by multi-port configurations becomes even more critical for preventing "dead zones" and ensuring uniform regeneration. Consequently, utilizing

multi-port strategies, specifically 2-M&B or 2-T&M, is not only beneficial for lab-scale efficiency but is also a necessary design criterion for upscaling to high-efficiency industrial VPSA plants.

References

1. IEA, Global Energy Review (2025). CO_2 Emissions in 2024 (International Energy Agency, Paris, 2025)
2. C.A. Grande (2012). Pressure swing adsorption after 40 years: Innovations and new applications. ISRN Chem. Eng., 2012, 673750.
3. P.A. Webley, A. Qader, A. Ntiamoah, J. Ling, P. Xiao, Y. Zhai (2017). CO_2 capture by vacuum pressure swing adsorption (VPSA) from flue gas – Performance and cost of carbon capture. *Energy Procedia*, 114, 2467-2472.
4. J. Yu, Y. Wang (2016). Optimization of a VPSA process for CO_2 capture from flue gas. *Ind. Eng. Chem. Res.*, *55* (11), 3060–3069.
5. J.-H. Lin, S. Wait, T.N. Pham, P. Halder, et al. (2021). Sustainable production of high-value carbon nanomaterials from plastic waste and biomass. Science, 374 (6574), 1464–1471.
6. T.T.T. Nguyen, G.K.H. Shimizu, A. Rajendran (2023). Rapid evaluation of metal–organic frameworks for post-combustion CO_2 capture using a simplified VPSA cycle model. Chem. Eng. J., 452, 139550.
7. J.B. Siegel, H.G.W. Nevison, D.S. Sholl (2022). High-throughput screening of metal-organic frameworks for CO2 capture from flue gas using vacuum pressure swing adsorption. Chem. Eng. J., 430, 137326.
8. R. Gutierrez-Ortega, N. Nomen, J. Sempere, J.B. Parra, M.A. Montes-Morán, R. Gonzalez-Olmosa (2022). Evaluation of commercial zeolites for CO_2 capture from flue gas by vacuum pressure swing adsorption. Chem. Eng. J., 435, 134703.
9. N. Henrotin, N. Heymans, M.E. Duprez, G. Mouchaham, C. Serre, D. Wong, G. De Weireld (2024). Evaluation of MOFs and zeolites for CO_2 capture from flue gas by vacuum pressure swing adsorption: A comparative study. Carbon Capture Sci. Technol., 12, 100224.
10. S. Cavenati, C.A. Grande, A.E. Rodrigues (2004). Adsorption equilibrium of methane, carbon dioxide, and nitrogen on zeolite 13X at high pressures. Microporous Mesoporous Mater., 74, 95–104.
11. H. Yang, Z. Xu, M. Fan, R. Gupta, R.B. Slimane, A.E. Bland, I. Wright (2008). Progress in carbon dioxide separation and capture: A review. J. Environ. Sci., 20, 14–27.
12. F.V.S. Lopes, C.A. Grande, A.E. Rodrigues (2011). Adsorption of H_2, CO_2, CH_4 and CO on zeolite 13X and activated carbon. Ind. Eng. Chem. Res., 50 (14), 8703–8710.
13. D.M. Ruthven, Principles of Adsorption and Adsorption Processes (John Wiley & Sons, New York, 1984)
14. Y.H. Yoon, J.H. Nelson (1984). Application of gas adsorption kinetics I. A theoretical model for respirator cartridge service life. Am. Ind. Hyg. Assoc. J., 45 (8), 509–516.